Electronic Supplementary Information (ESI) for Dalton Transactions

Accompanying the manuscript

Synthesis, characterization, DNA interaction and cleavage, and *in vitro* cytotoxicity of copper(II) mixed-ligand complexes with 2-phenyl-3-hydroxy-4(1*H*)-quinolinone

Roman Buchtík [a], Zdeněk Trávníček [b*], Ján Vančo [b], Radovan Herchel [a], Zdeněk Dvořák [c]

[a] *Department of Inorganic Chemistry, Faculty of Science, Palacký University, 17. listopadu 12, CZ-771 46 Olomouc, Czech Republic*

[b] *Regional Centre of Advanced Technologies and Materials, Department of Inorganic Chemistry, Faculty of Science, Palacký University, 17. listopadu 12, CZ-771 46 Olomouc, Czech Republic*

[c] *Regional Centre of Advanced Technologies and Materials, Department of Cell Biology and Genetics, Faculty of Science, Palacký University, Šlechtitelů 11, CZ-783 71 Olomouc, Czech Republic*

[*] Corresponding author. Tel.: +420 585 634 352; fax: +420585 634 954; e-mail: zdenek.travnicek@upol.cz (Zdeněk Trávníček).

List of Contents:

S-1: General methods used and synthesis of the Cu(II) complexes 1–6

Materials. Chemicals and solvents were purchased from Sigma-Aldrich Co., Lachema Co. or Fluka Co. and were used as received.

Elemental Analysis. Elemental analysis (C, H, N) was performed on a Flash EA-2000 Elemental Analyser (ThermoFisher Scientific).

Conductivity. Molar conductivity measurements were carried out on a Cond 340i/SET (WTW) in *N,N′*-dimethylformamide (DMF; 10^{-3} M) solutions at 25 °C.

UV-Vis Spectroscopy. Electronic absorption spectra of 10^{-3} M DMF solutions and diffuse-reflectance spectra were recorded with a Lambda 40 spectrometer (Perkin Elmer instruments) in the range of 300–1000 nm.

Infrared Spectroscopy. FTIR spectra were recorded on a Nexus 670 FTIR (ThermoNicolet) using KBr (400–4000 cm^{-1}) and Nujol (150–600 cm^{-1}) techniques.

Raman Spectroscopy. Raman spectroscopy measurements were performed on an NXR FT-Raman Module (ThermoNicolet) in the range of 150–3750 cm^{-1}.

Mass Spectrometry. Mass spectrometry studies were performed on an LTQ Fleet (ThermoFisher Scientific) with the ESI+ full scan mode in 10^{-5} M methanolic solutions.

Thermogravimetry. Simultaneous thermogravimetric (TG) and differential thermal (DTA) analyses were carried out using a thermal analyzer Exstar TG/DTA 6200 (Seiko Instruments Inc.). TG/DTA studies were performed in platinum pans from laboratory temperature to 600 °C with a 2.5 °C min^{-1} temperature gradient in dynamic air atmosphere (100 mL min^{-1}).

Magnetic measurements. The magnetic measurements were performed on an MPMS XL-7 Quantum Design SQUID magnetometer in the temperature range of 2–300 K with an applied field of 1 T and the isothermal magnetizations were measured at $T = 2.0$ and 4.6 K up to magnetic field of $B = 7$ T. The acquired data were corrected for the diamagnetism using Pascal's constants and the temperature independent paramagnetism (TIP) χ_{TIP} =

$0.75 \cdot 10^{-9}$ m^3 mol^{-1} for the Cu(II) ion was used as well.[1]

EPR Spectroscopy. EPR spectra were recorded on a MiniScope MS200 spectrometer (Magnettech) at liquid nitrogen temperature (~77 K); TEMPONE (4-oxo-2,2,6,6-tetramethylpiperidine-N-oxyl) was used as a standard.[2]

X-ray measurements. X-ray data of suitable single crystals of **2**, **3a** and **Hqui** were collected on an Xcalibur™2 diffractometer (Oxford Diffraction Ltd.) with Mo Kα (Monochromator Enhance, Oxford Diffraction Ltd.) and Sapphire2 CCD detector at 120 K, and 105 K, respectively. Data collection and reduction were performed using CrysAlis software (Version 1.171.33.52).[3] Structures were solved by direct methods using SHELXS-97 and refined on F^2 using the full-matrix least-squares procedure.[4] Non-hydrogen atoms were refined anisotropically. All hydrogen atoms, were found from differential Fourier maps and refined using the riding model, with C–H = 0.95 Å, N–H = 0.88 Å, and Uiso(H) = 1.2Ueq. The H1V atom belonging to the crystal water molecule of **2** is disordered over two positions with the occupancy factors of 0.63 (for H1V) and 0.37 (for H1U). The molecular graphics was drawn and additional structural parameters were interpreted using DIAMOND.[5]

Synthesis of 2-phenyl-3-hydroxy-4(1H)-quinolinone

2-Phenyl-3-hydroxy-4(1*H*)-quinolinone (Hqui) was synthesized accordingly to the method described previously.[6] The compound was characterized by elemental analysis and FTIR (Found: C, 75.6; H, 4.3; N, 5.7. $C_{15}H_{11}NO_2$ requires C, 75.9; H, 4.7; N, 5.9%). FTIR (ν, cm^{-1}): 3066br and 2942br (CH), 1631vs (CO), 1550vs and 1489vs (CC_{ar}), 1368vs (CNH), 1269vs, 1149s, 758s, 692s, 518m. The X-ray structure of Hqui was determined, for crystal data and structure refinement (Table S1), selected interatomic parameters (Table S2), and figures of molecular and crystal structures (Figs. S1 and S2).

[1] E. König, Landolt-Börstein, Springer, Berlin, 1966.
[2] W. Snipes, J. Cupp, G. Cohn, A. Keith, *Biophys. J.*, 1974, **14**, 20.
[3] CrysAlis CCD and CrysAlis RED, Version 1.171.33.52, Oxford Diffraction Ltd., England, 2009.
[4] G.M. Sheldrick, *Acta Crystallogr., Sect. A*, 2008, **64**, 112.
[5] K. Brandenburg, DIAMOND, Relase 3.1f, Crystal Impact GbR, Bonn, Germany, 2006.
[6] P. Hradil, J. Jirman, *Collect. Czech. Chem. Commun.*, 1995, **60**, 1357.

General Synthetic Procedure for the Cu(II) Complexes 1–6

To a solution of 2-phenyl-3-hydroxy-4(1*H*)-quinolinone (237 mg, 1 mmol) in ethanol (50 mL), the corresponding bidentate N-donor ligand (L) (1 mmol) in EtOH (5 mL) was added while stirring. To this mixture, a solution of $Cu(NO_3)_2 \cdot 3H_2O$ (242 mg, 1 mmol) in H_2O (5 mL) was dropped while stirring. The reaction mixture was stirred at room temperature for a few hours, and then, it was left to stand for several days. A formed crystalline product was collected by filtration, washed with a small amount of cold ethanol and dried at 40 °C under infrared lamp.

[Cu(qui)(bpy)]$NO_3 \cdot 1/2H_2O$ (**1**). (347 mg, 67%), (Found: C, 57.0; H, 3.4.; N, 10.5. $C_{25}H_{19}CuN_4O_{5.5}$ requires C, 57.0; H, 3.6; N, 10.6%). FTIR (ν, cm^{-1}): 3502br (OH), 3063br (CH), 1627m (CO), 1562m and 1490w (CC_{ar}), 1373vs (CNH), 1309vs (NO_3), 1036m, 756s, 730m, 544w, 494w, 342w. Raman (ν, cm^{-1}): 3079m (CH), 2927w (CH), 1600vs (CO), 1513m (CC_{ar}), 1398s, 1325m (NO_3), 1173m, 1040m, 1000m, 580w, 284w. ESI+MS: m/z 455 ($[M–NO_3]^+$, 100%). TG/DTA: weight loss of 1.1% found in the region of 26–79 °C (1.7% calcd. for $1/2H_2O$); decomposition began at 179 °C and finished at 385 °C with a weight loss of 83.4% (83.2% calcd. for CuO residue). Λ_m (S cm^2 mol^{-1}): 70 (electrolyte 1:1).

[Cu(qui)(phen)]$NO_3 \cdot H_2O$ (**2**). Single crystals of **2** (304 mg, 55%) were obtained from the ethanolic mother liquor after standing for three weeks, (Found: C, 57.5; H, 3.6; N, 9.9. $C_{27}H_{20}CuN_4O_6$ requires C, 57.9; H, 3.6; N, 10.0%). FTIR (ν, cm^{-1}): 3458br (OH), 3063br (CH), 1629m (CO), 1563m and 1487s (CC_{ar}), 1370vs (CNH), 1317vs (NO_3), 1036m, 761w, 716s, 542w, 493w, 341w. Raman (ν, cm^{-1}): 3068s (CH), 1603vs (CO), 1455s (CC_{ar}), 1396vs, 1323s (NO_3), 1174m, 1000s, 743m, 582w, 434w, 283w. ESI+MS: m/z 479 ($[M–NO_3]^+$, 100%). TG/DTA data: weight loss of 3.1% found in the region of 26–148 °C (3.3% calcd. for H_2O); decomposition began at 197 °C and finished at 417 °C with a weight loss of 83.2% (84.0% calcd. for CuO residue). Λ_m (S cm^2 mol^{-1}): 68 (electrolyte 1:1).

[Cu(qui)(ambpy)]$NO_3 \cdot 1/2H_2O$ (**3**). (320 mg, 59%), (Found: C, 55.2; H, 3.5; N, 12.7. $C_{25}H_{20}CuN_5O_{5.5}$ requires C, 55.4; H, 3.7; N, 12.9%). FTIR (ν, cm^{-1}): 3473br (OH), 3145m (NH), 3047br (CH), 1649s, 1631s (CO), 1568s and 1488vs (CC_{ar}), 1374vs (CNH), 1325s (NO_3), 1013m, 760s, 543w, 495w, 336w. ESI+MS: m/z 470 ($[M–NO_3]^+$, 100%).

TG/DTA: weight loss of 1.9% found in the region of 26–180 °C (1.7% calcd. for H_2O); decomposition began at 180 °C and finished at 467 °C with a weight loss of 83.7% (83.7% calcd. for CuO residue). Λ_m (S cm^2 mol^{-1}): 71 (electrolyte 1:1). Non-hydrated single crystals (**3a**) were obtained from the mother liquor after four weeks standing at ambient temperature.

[Cu(qui)(mphen)]NO_3·H_2O (**4**). (372 mg, 65%), Found: C, 58.7; H, 3.8; N, 9.6. $C_{28}H_{22}CuN_4O_6$ requires C, 58.6; H, 3.9; N, 9.8%. FTIR (ν, cm^{-1}): 3414br (OH), 3070br (CH), 1629s (CO), 1566m and 1488s (CC_{ar}), 1373vs (CNH), 1317vs (NO_3), 1040w, 906w, 766m, 543w, 496w, 344w. Raman (ν, cm^{-1}): 3066m (CH), 2927w (CH), 1600vs (CO), 1519m (CC_{ar}), 1468m (CC_{ar}), 1400s, 1327m (NO_3), 1178m, 1000m, 580w, 434w, 289w. ESI+MS: m/z 493 ($[M–NO_3]^+$, 100%). TG/DTA: weight loss of 2.8% found in the region of 26–143 °C (3.1% calcd. for H_2O); decomposition began at 193 °C and finished at 431 °C with a weight loss of 82.4% (83.0% calcd. for CuO residue). Λ_m (S cm^2 mol^{-1}): 70 (electrolyte 1:1).

[Cu(qui)(nphen)]NO_3·H_2O (**5**). (425 mg, 70%), (Found: C, 53.6; H, 2.9; N, 11.5. $C_{27}H_{19}CuN_5O_8$ requires C, 53.6; H, 3.2; N, 11.6%. FTIR (ν, cm^{-1}): 3414br (OH), 3082br, (CH), 1631m (CO), 1563s and 1485vs (CC_{ar}), 1373vs (CNH), 1327vs (NO_3), 1039w, 913w, 840m, 762m, 546w, 496w, 339w. Raman (ν, cm^{-1}): 3079m (CH), 1600vs (CO), 1564m (CC_{ar}), 1458s (CC_{ar}), 1397s, 1346, 1327m (NO_3), 1259m, 1170m, 1000m, 580w, 290w. ESI+MS: m/z 524 ($[M–NO_3]^+$, 100%). TG/DTA: weight loss of 2.7% found in the region of 69–117 °C (3.0% calcd. for H_2O); decomposition began at 177 °C and finished at 394 °C with a weight loss of 84.0% (83.9% calcd. for CuO residue). Λ_m (S cm^2 mol^{-1}): 71 (electrolyte 1:1).

[Cu(qui)(bphen)]NO_3·H_2O (**6**). (478 mg, 67%), (Found: C, 66.3, H, 4.2; N, 7.7. $C_{39}H_{28}CuN_4O_6$ requires C, 65.8; H, 4.0; N, 7.9%. FTIR (ν, cm^{-1}): 3423br (OH), 3060br (CH), 1628vs (CO), 1562vs and 1488vs (CC_{ar}), 1371vs (CNH), 1318vs (NO_3), 1035w, 857m, 761s, 733s, 699s, 545m, 494w, 340w. Raman (ν, cm^{-1}): 3061s (CH), 1600w (CO), 1514w (CC_{ar}), 1437w (CC_{ar}), 1400w, 1321w (NO_3), 1289w, 1159w, 1000w. ESI+MS: m/z 631 ($[M–NO_3]^+$, 100%). TG/DTA: weight loss of 3.9% found in the region of 26–161 °C (3.7% calcd. for H_2O); decomposition began at 211 °C and finished at 519 °C with a weight loss of 85.5% (86.3% calcd. for CuO residue). Λ_m (S cm^2 mol^{-1}): 65 (electrolyte

1:1).

S-2: X-ray characterization of Hqui

Crystallographic data for Hqui dimethyl sulfoxide (DMSO) solvate was described in lit.[7] Herein, we present the molecular and crystal structure of the unsolvated form of Hqui.

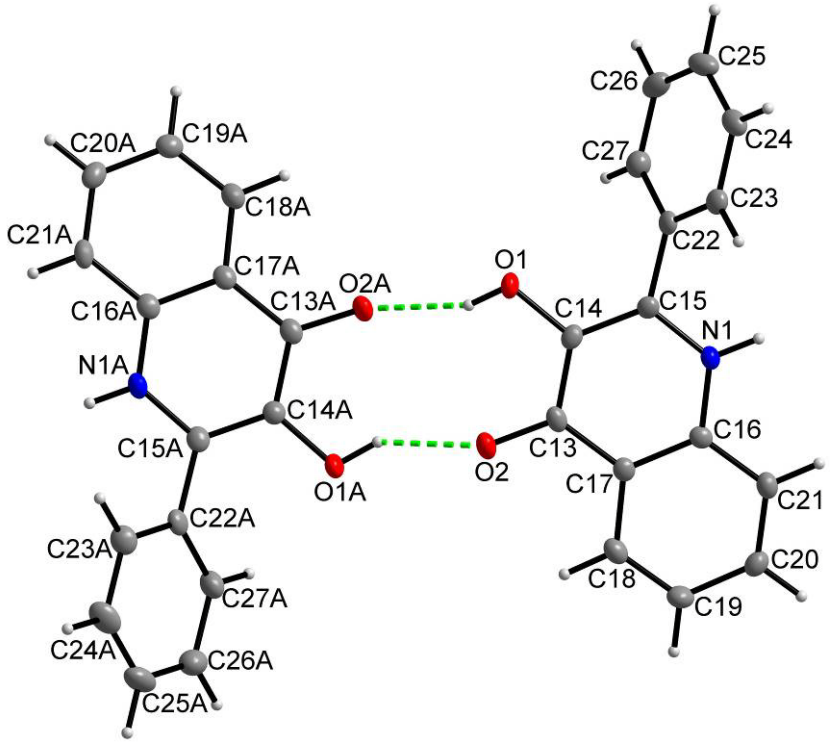

Figure S1. Molecular structure of Hqui together with the atom numbering scheme, showing the two crystallographically independent molecules. The non-H atoms are drawn as thermal ellipsoids at the 50% probability level. The O−H···O hydrogen bonds are shown as dashed green lines.

[7] M. Czaun, I. Gansky, G. Speier, L. Parkanyi, *Z. Kristallogr. - New Cryst. Struct.*, 2002, **217**, 379.

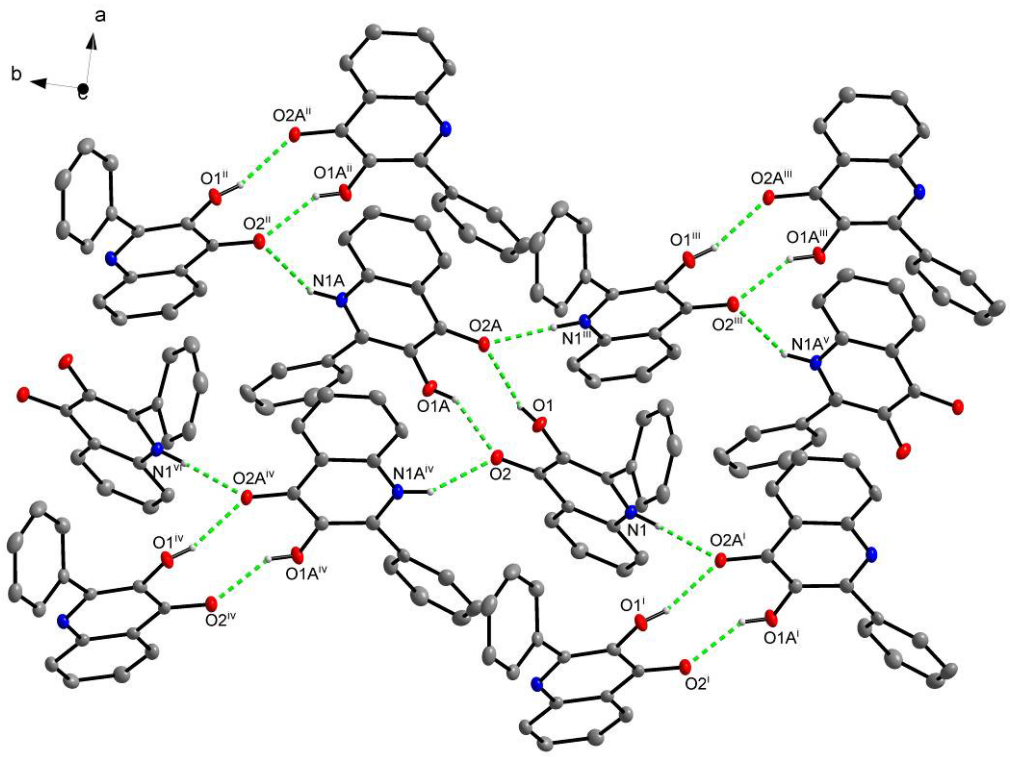

Figure S2. A part of the crystal structure of Hqui showing the N−H···O and O−H···O hydrogen bonds (dashed green lines). The H–atoms not involved in the interactions were omitted for clarity. Symmetry codes: (i) –0.5 + x, 0.5 – y, z; (ii) 0.5 + x, 1.5 – y, z; (iii) 0.5 + x, 0.5 – y, z; (iv) –0.5 + x, 1.5 – y, z; (v) x, –1 + y, z; (vi) x, 1 + y, z.

S-3: List of supplemental figures of the Cu(II) complexes 1–6

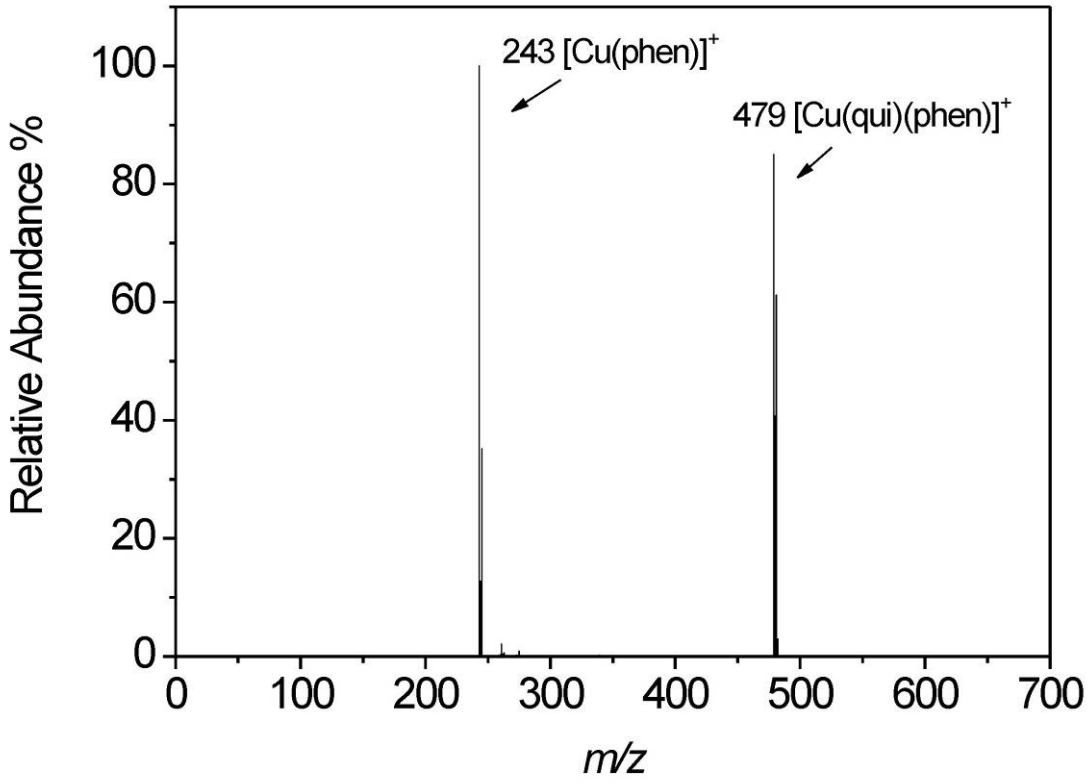

Figure S3. ESI+ MS^2 spectrum of complex **2**, showing the fragmentation pattern of parent ion 479 *m/z* corresponding to $[Cu(qui)(phen)]^+$ and its fragmentation to the 243 *m/z* ion, corresponding to the $[Cu(phen)]^+$ species.

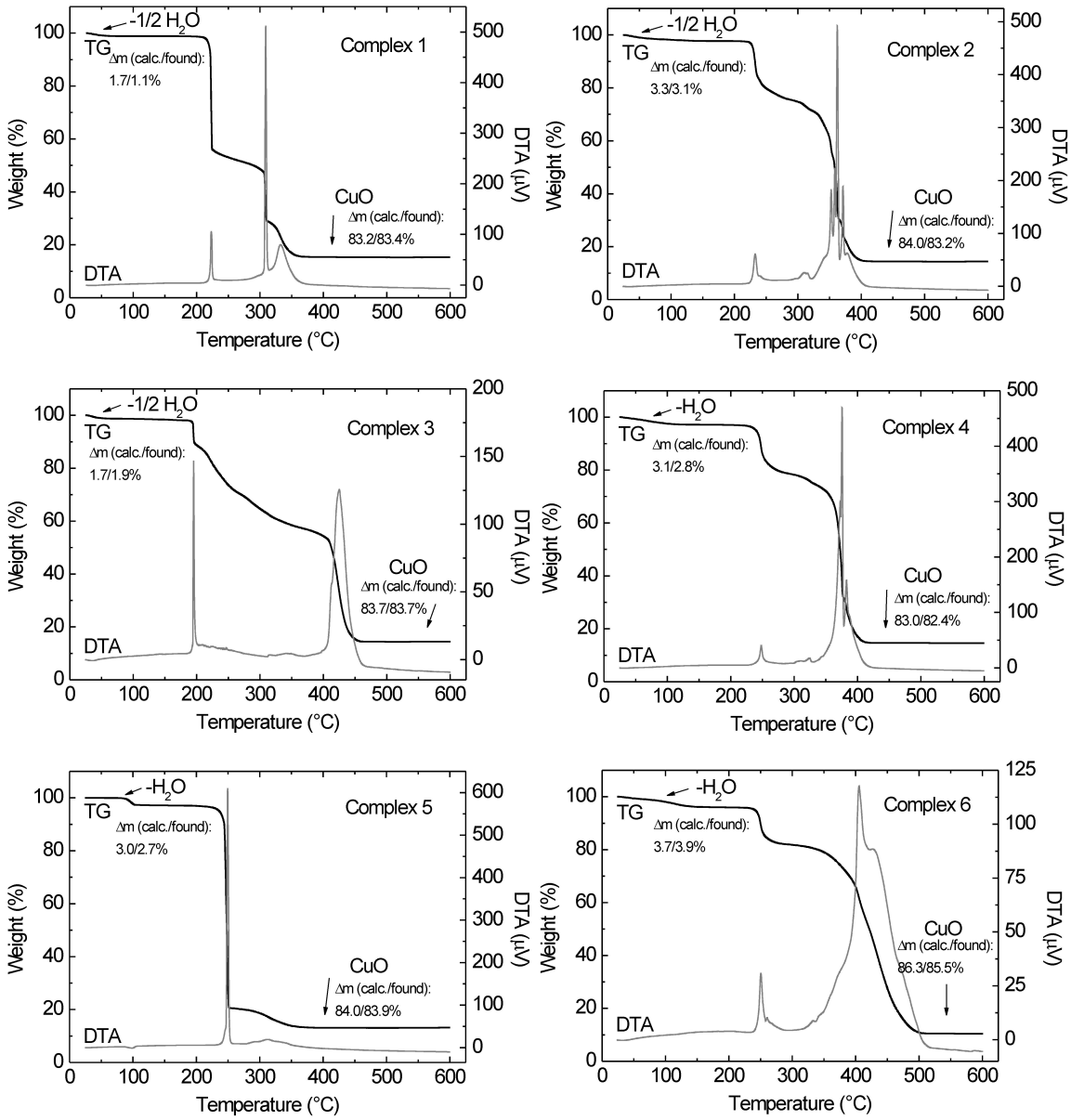

Figure S4. TG/DTA curves of Cu(II) complexes **1**–**6**, showing the course of thermal degradation of the corresponding complex together with crystal water elimination and final product formation.

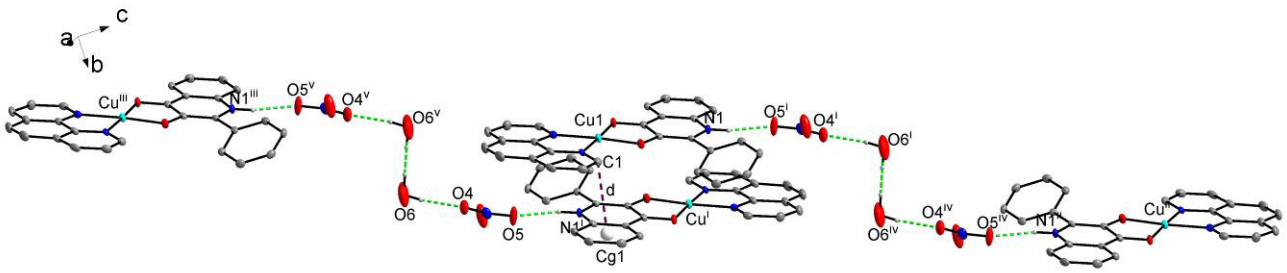

Figure S5. A part of the crystal structure of complex **2** showing the π–π stacking between two molecules of the complex; Cg1···C1 distance (d) is equal to 3.338(2) Å (dashed violet line), where Cg1 is defined as a centroid of the quinoline aromatic ring of the first molecule and C1 is the carbon atom of phen of the second one. Dimers are connected via the N–H···O and O–H···O hydrogen bonds (dashed green lines). The H–atoms not involved in the interactions are omitted for clarity. Symmetry codes: (i) 1 – x, 1 – y, 2 – z; (ii) 1 – x, 2 – y, 3 – z; (iii) x, –1 + y, –1 + z ; (iv) x, 1 + y, 1 + z; (v) 1 – x, –y, 1 – z.

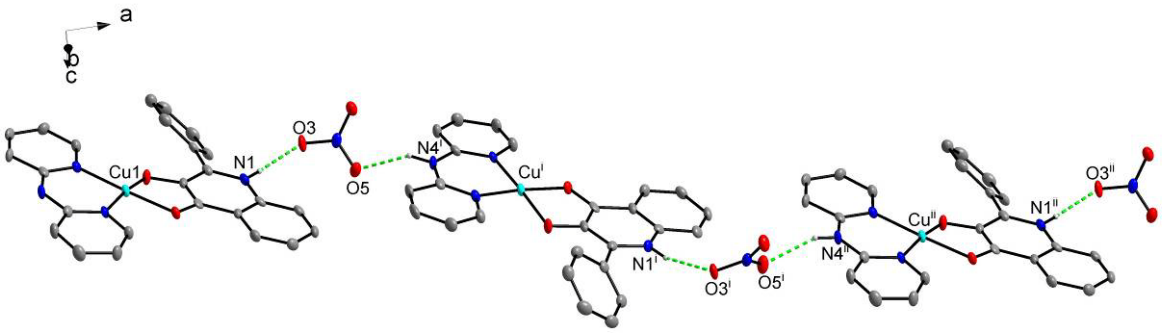

Figure S6. A part of the crystal structure of complex **3a** showing the N−H···O hydrogen bonds (green dashed lines). The H–atoms not involved in the interactions are omitted for clarity. Symmetry codes: (i) 1 + x, 1 – y, 0.5 + z; (ii) 2 + x, y, 1 + z; (iii) x, y, 1 + z.

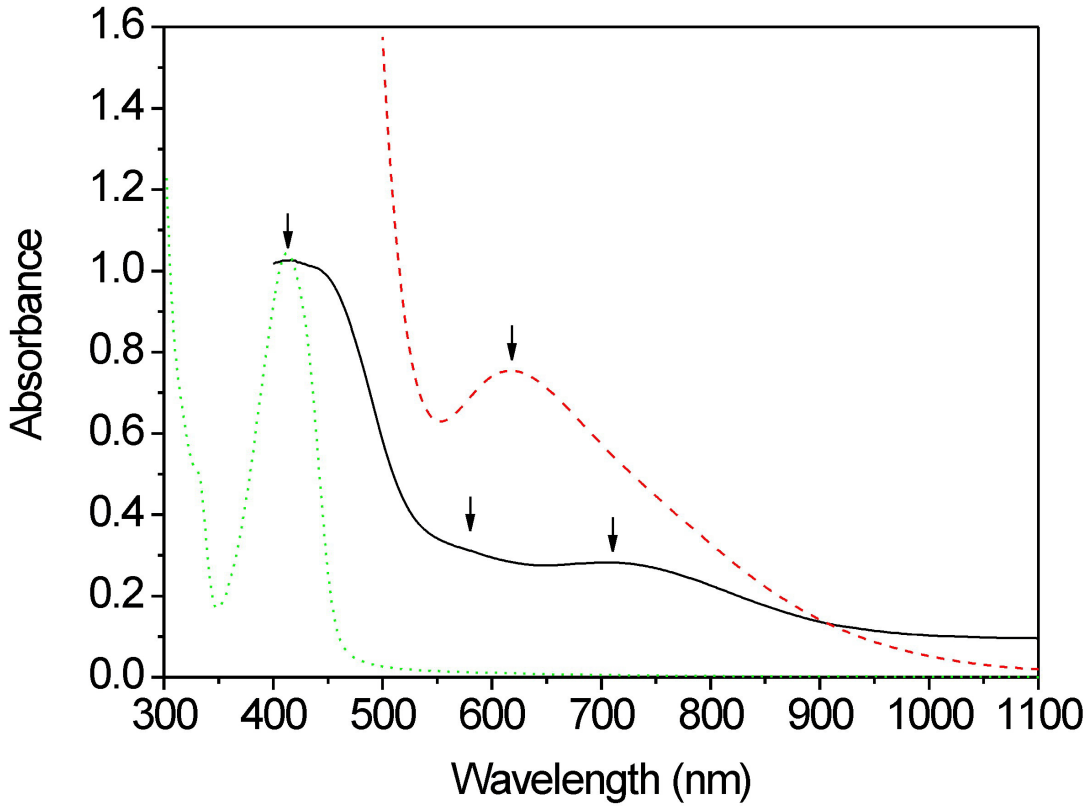

Figure S7. Electronic spectra of complex **2**. Solid state spectrum with maxima at 416 nm, 584 nm and 707 nm (black line); 10^{-2} M DMF solution spectrum with a maximum at 617 nm (red dashed line), $\varepsilon = 151$ M^{-1} cm^{-1}; 10^{-4} M DMF solution spectrum with a maximum at 416 nm (green dotted line) $\varepsilon = 37800$ M^{-1} cm^{-1}. Maxima displayed as black arrows.

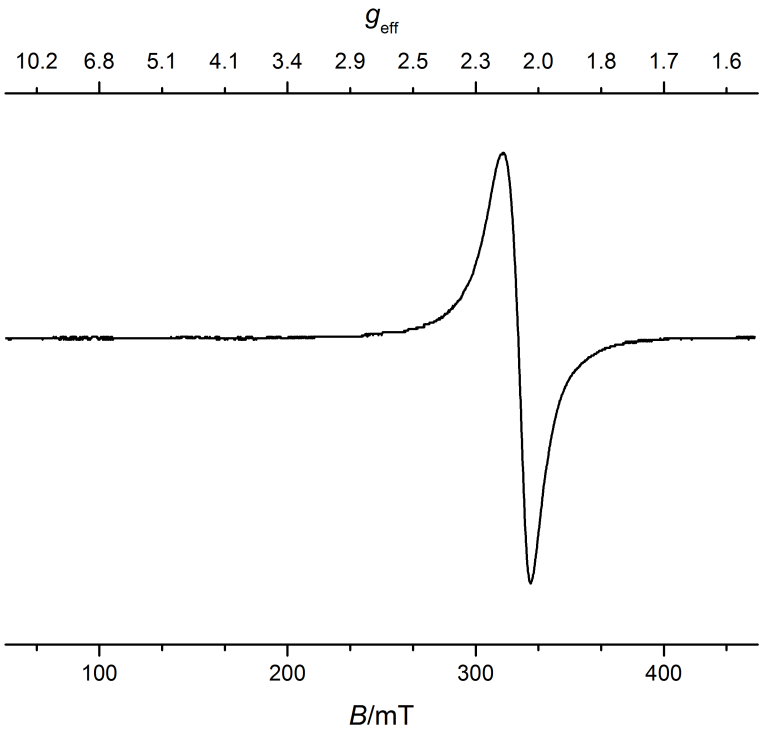

Figure S8. Powder X-band EPR spectrum of complex **2** measured at 77 K.

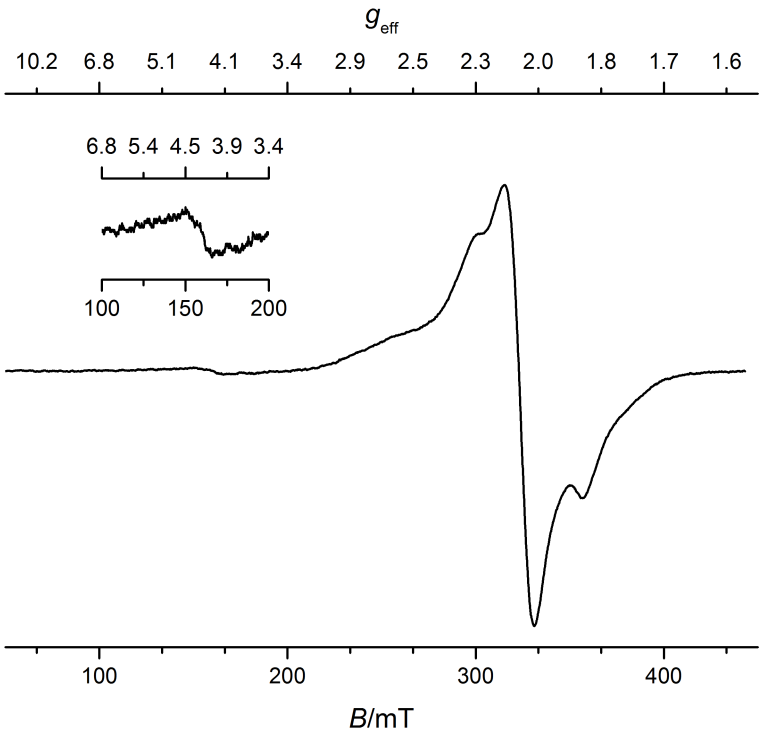

Figure S9. Powder X-band EPR spectrum of complex **1** measured at 77 K. Inset: the magnified region (26x) of $\Delta M_S = \pm 2$ transitions.

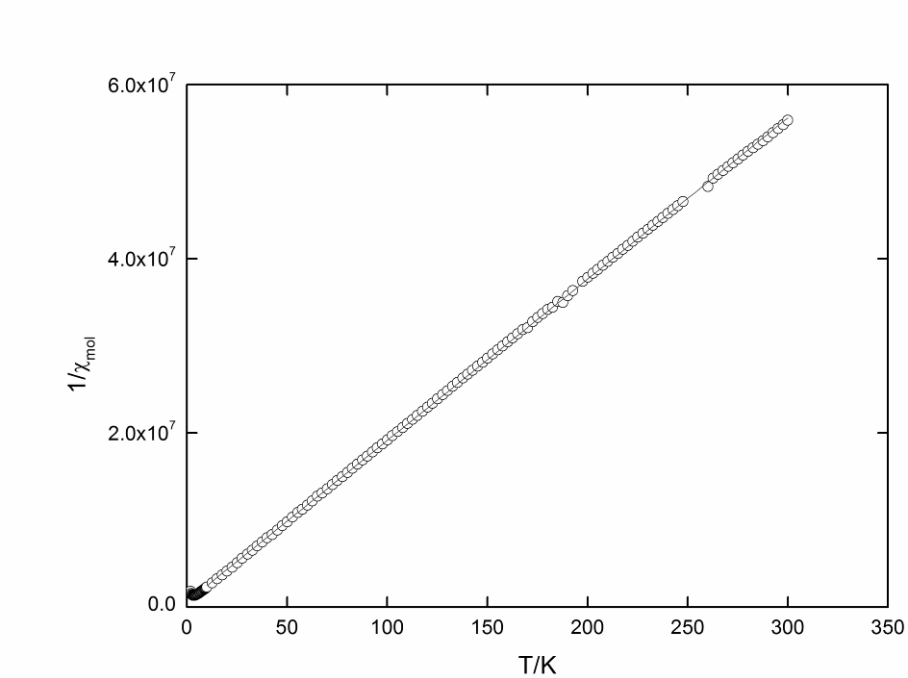

Figure S10. The inverse molar susceptibility of complex **1** (empty circles). The Curie-Weiss law fit for the temperature range of 10–300 K (full line), with $g = 2.14$ and $\Theta = -3.3$ K.

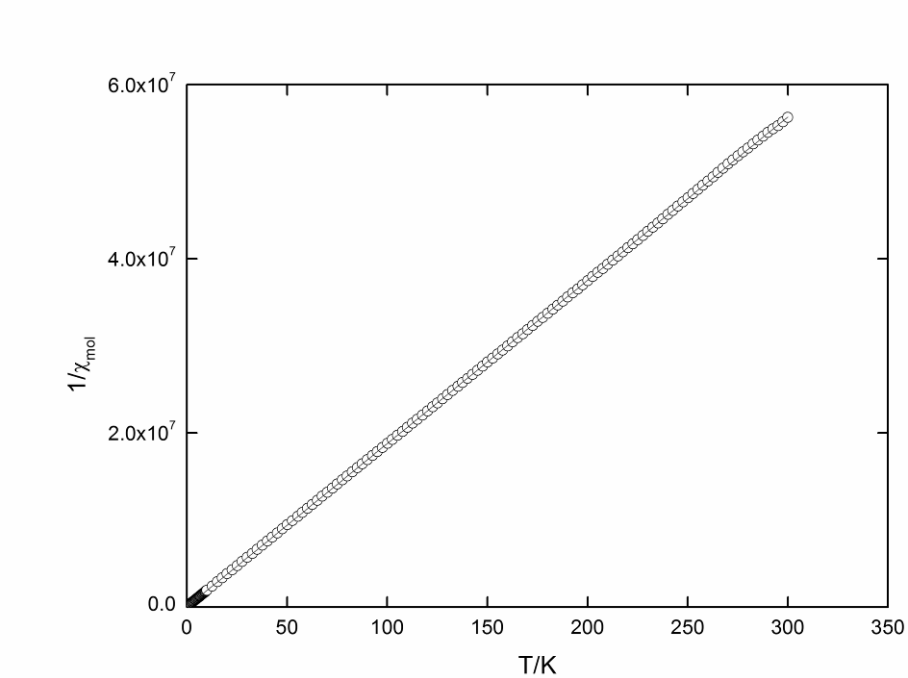

Figure S11. The inverse molar susceptibility of complex **2** (empty circles). The Curie-Weiss law fit for the temperature range of 2–300 K (full line), with $g = 2.13$ and $\Theta = -0.1$ K.

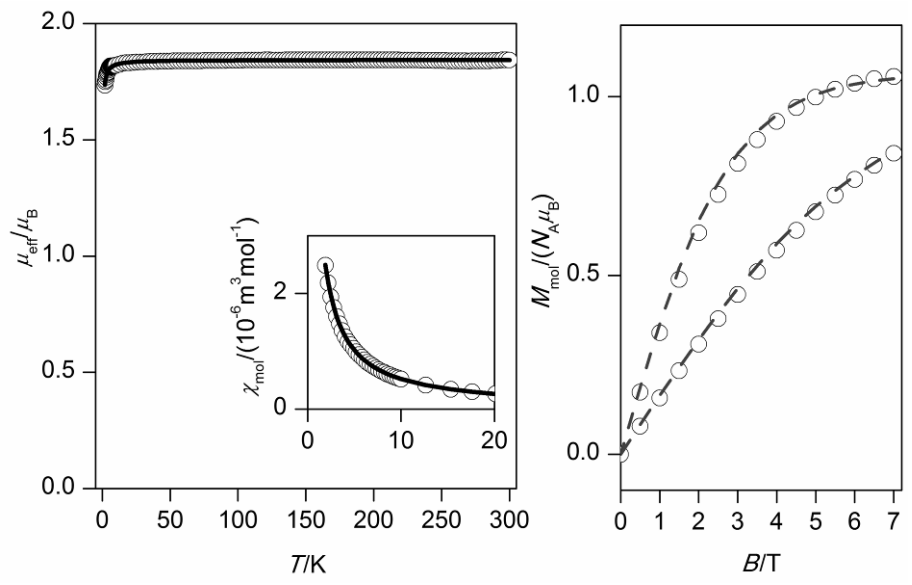

Figure S12. Magnetic data for complex **2** scaled per one Cu(II). *Left*: temperature dependence of the effective magnetic moment (calculated from the temperature dependence of magnetization at B =1 T). *Inset*: temperature dependence of the molar susceptibility with empty circles representing the experimental points. Full line: the best fit to the experimental data calculated using Johnston et al. equation, with $J = -0.30$ cm^{-1} and $g = 2.13$. *Right*: field dependence of magnetization at $T = 2.0$ and 4.6 K. Empty circles: experimental points. Dashed line: the Brillouin law for the isolated Cu(II) ion**.**

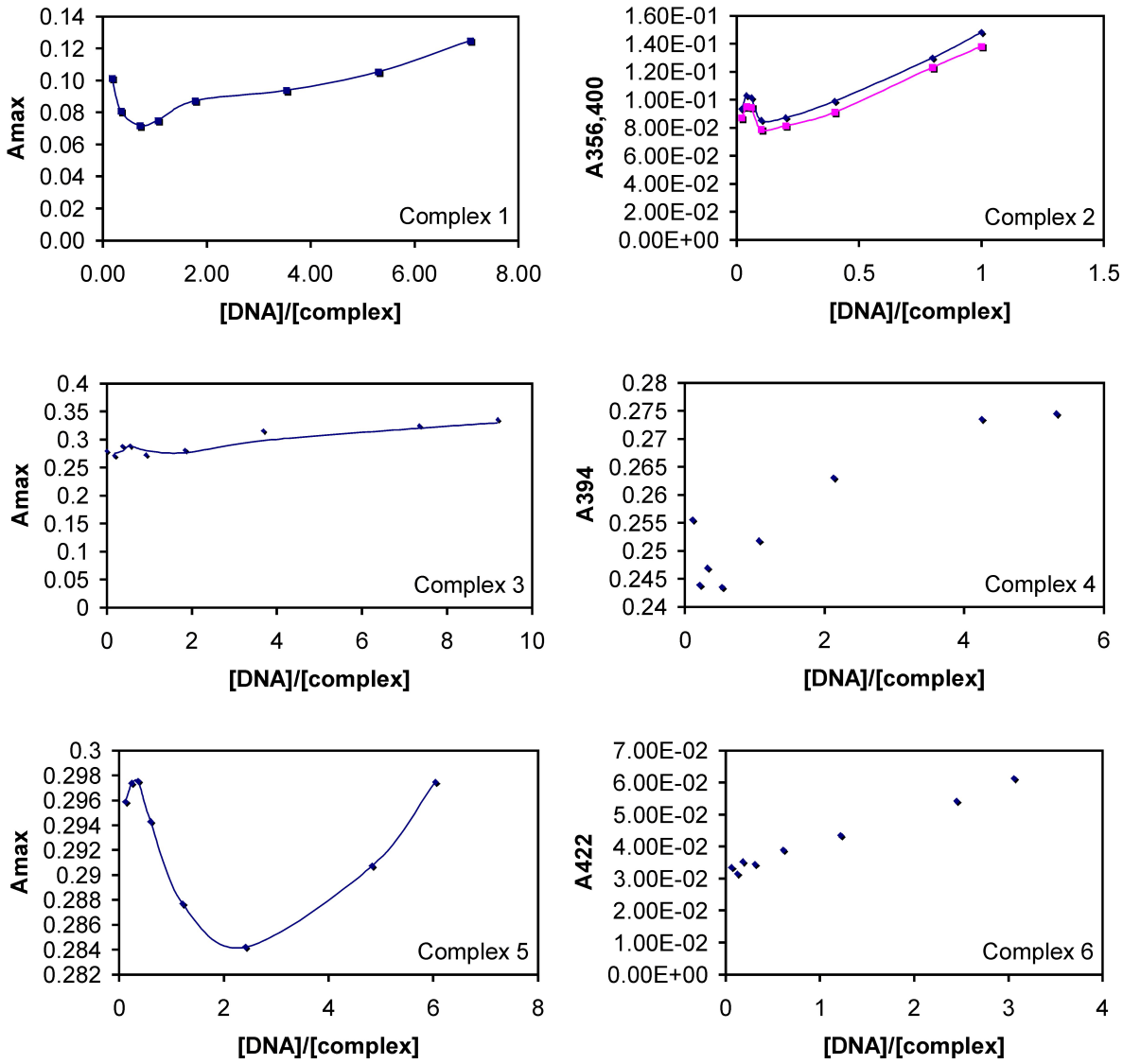

Figure S13. A plot of absorbance at the corresponding maximum of the charge-transfer transition *vs.* the [DNA]/[complex] molar ratio in the absorption spectra of complexes **1-6** (50 μM) binding to CT-DNA at different molar ratios.

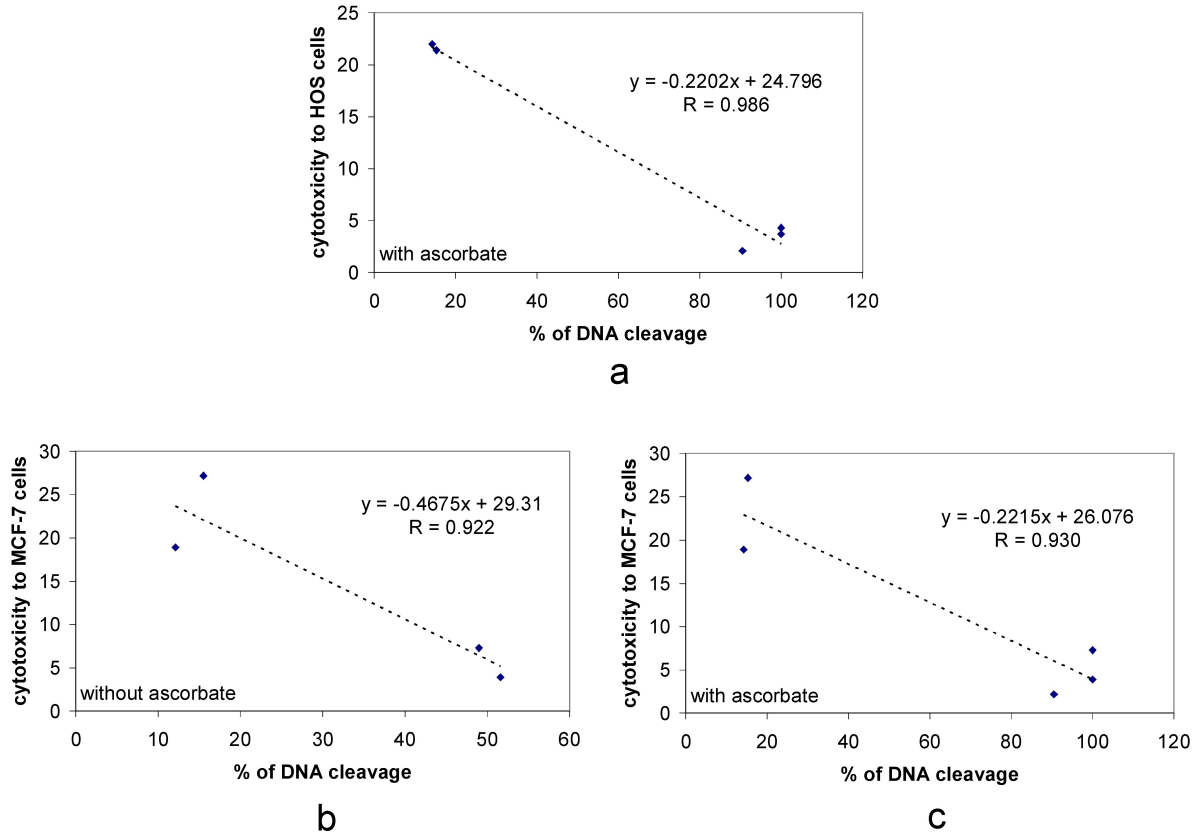

Figure S14. The correlation between the cytotoxicity to HOS cells vs. the percentage of DNA cleavage at 20μM with the addition of ascorbate (**a**); MCF-7 cells vs. the percentage of DNA cleavage at 20μM without the addition of ascorbate (**b**); MCF-7 cells vs. the percentage of DNA cleavage at 20μM with the addition of ascorbate (**c**).

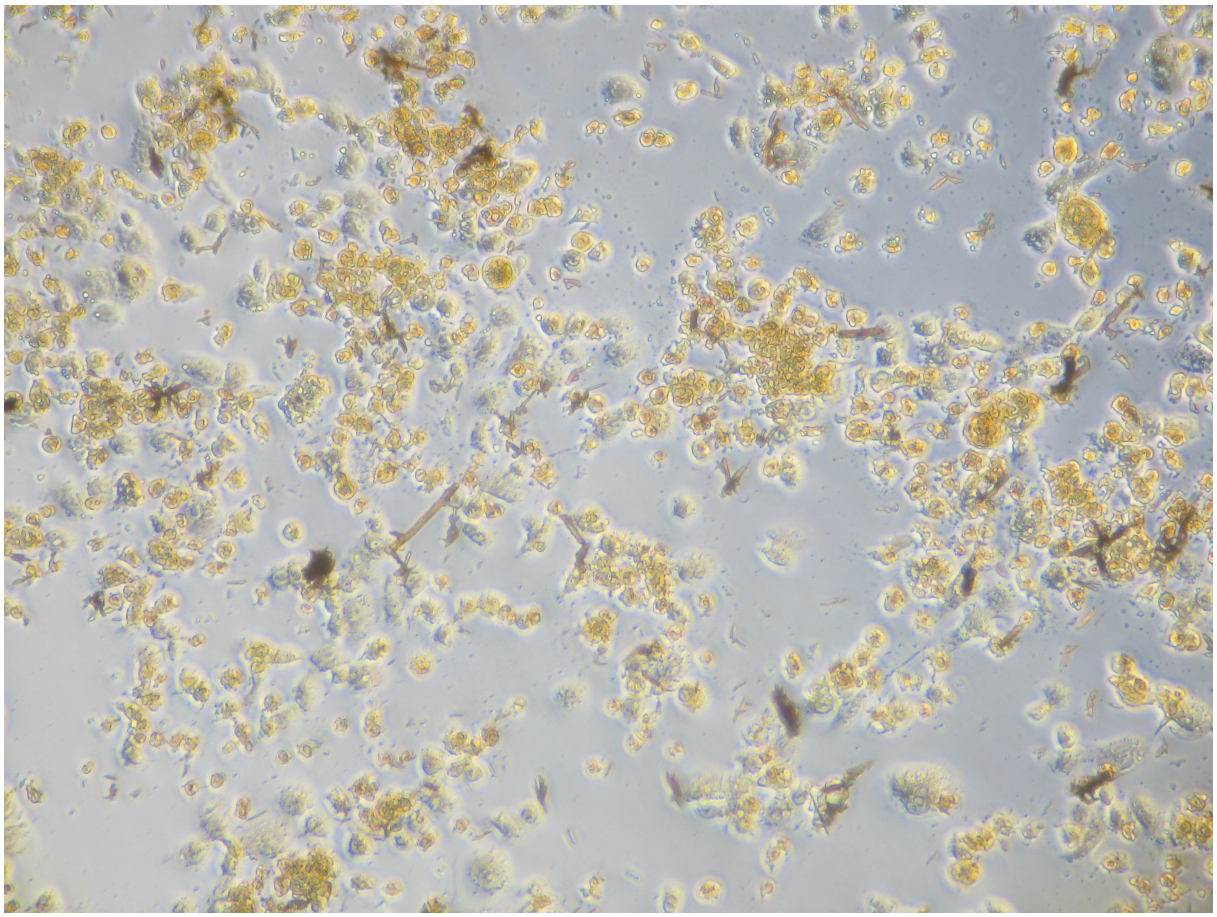

Figure S15. Visualization of intracellular copper in THP-1 cells cultured with complex **2** by the rhodanine method. The red-brown colour indicates the increased levels of copper inside the cells.

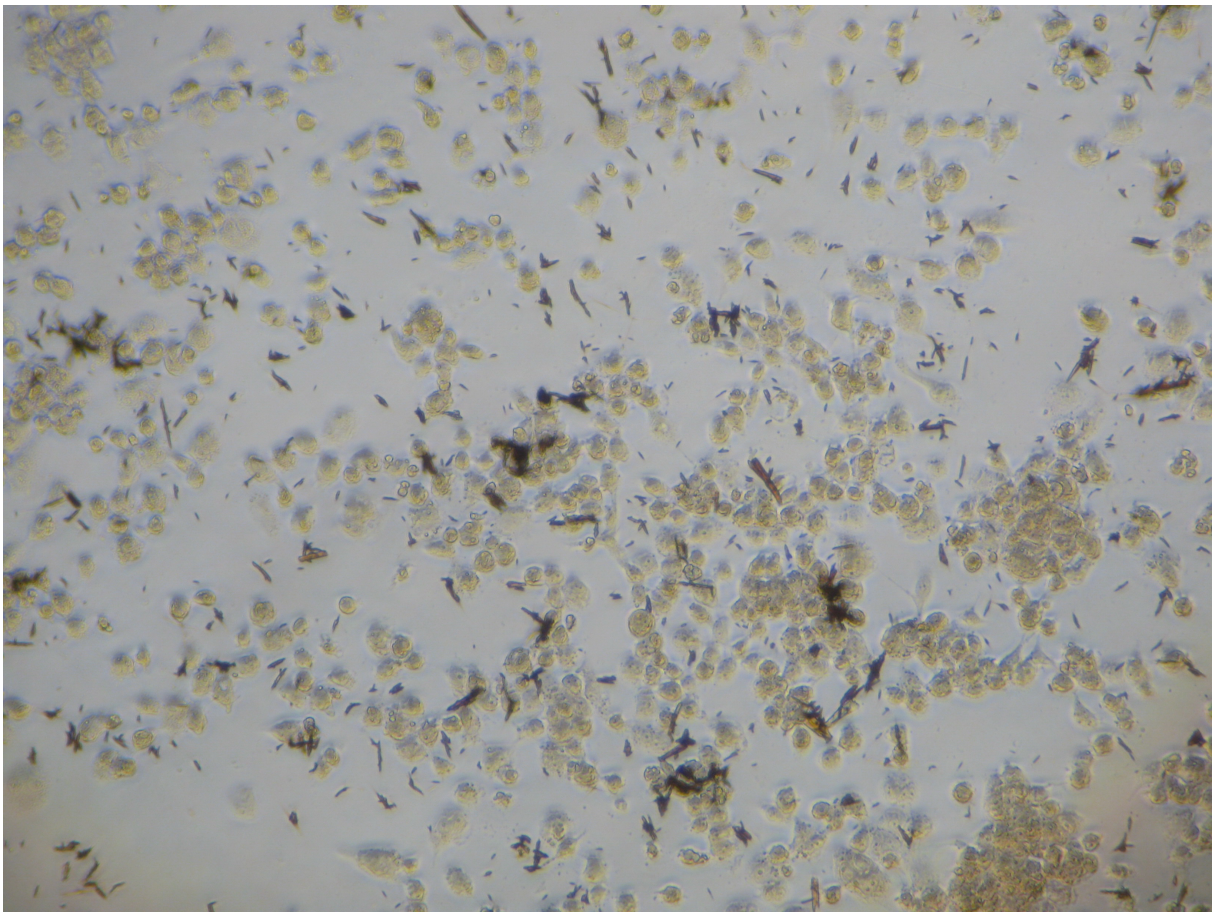

Figure S16. Staining of THP-1 cells cultured as blank by the rhodanine method.

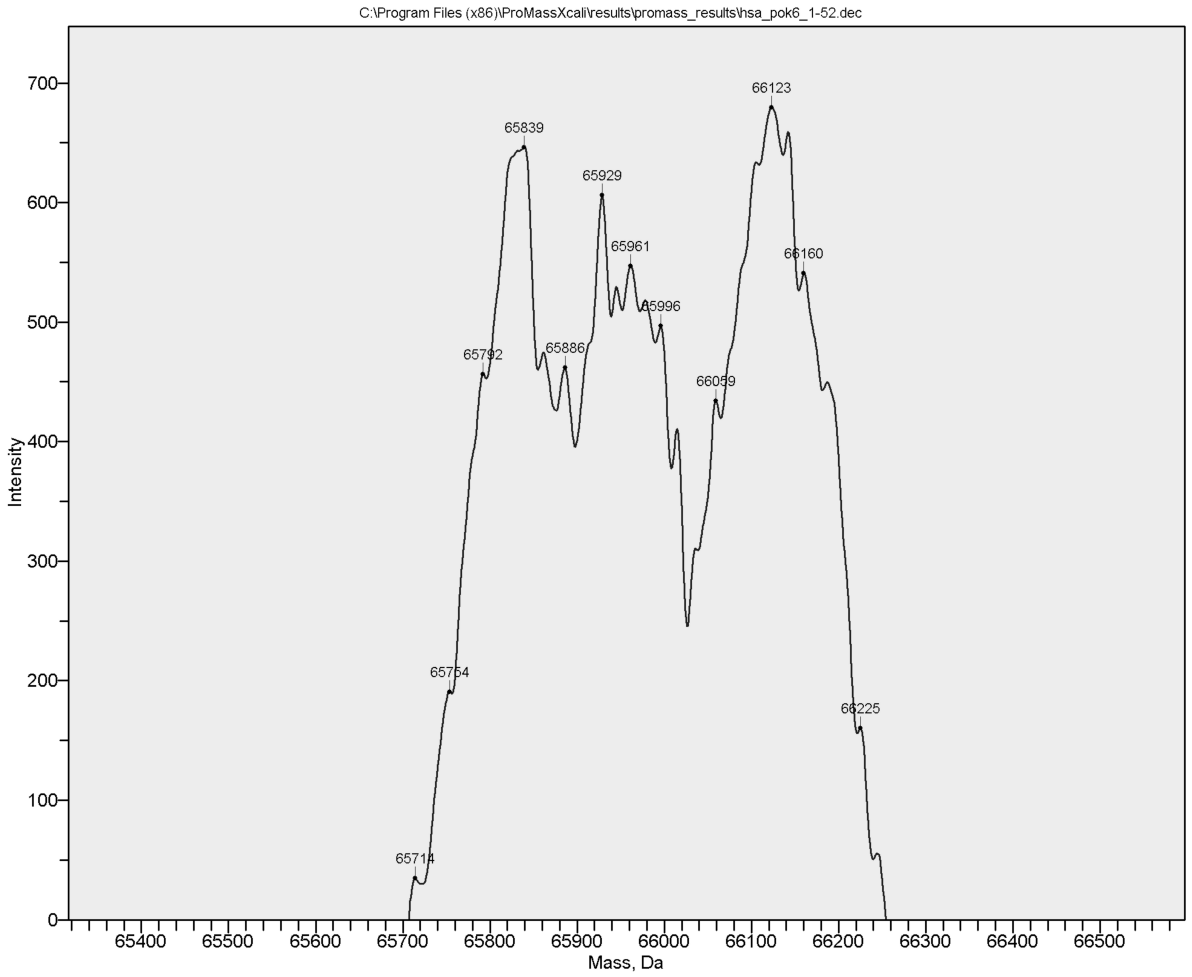

Figure S17. Deconvoluted ESI-MS spectrum of the mixture of complex **2** and HSA (human serum albumin) in molar ratio of 10:1, measured after 30 minutes of the reaction, showing on interaction of a complex with HSA (a maximum of 66 123 Da).

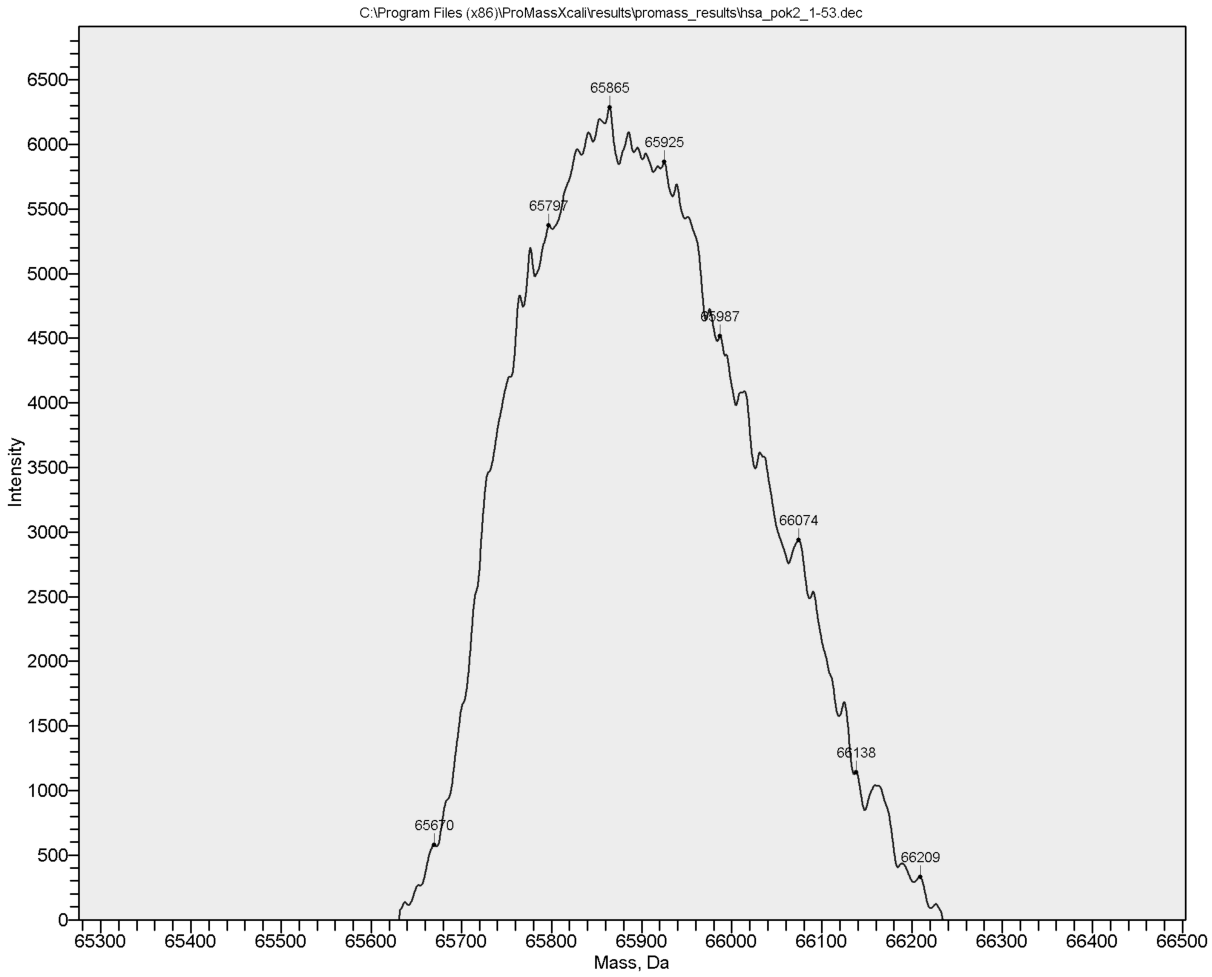

Figure S18. Deconvoluted ESI-MS spectrum of intact HSA, showing the mean mass of 65 865 Da.

S-4: List of supplemental tables of the Cu(II) complexes 1–6

Table S1. Crystal data and structure refinements for Hqui (2-phenyl-3-hydroxy-4(*1H*)-quinolinone)

Empirical formula	$C_{15}H_{11}NO_2$
Formula weight	237.25
Temperature (K)	100(2)
Wavelength (Å)	0.71073
Crystal system, space group	Orthorhombic, Pna21
Unit cell dimensions	
a (Å)	9.8636(3)
b (Å)	12.9003(4)
c (Å)	17.8871(6)
α (°)	90
β (°)	90
γ (°)	90
V (Å^3)	2276.02(12)
Z, D_{calc} (g cm^{-3})	8, 1.385
Absorption coefficient (mm^{-1})	0.093
Crystal size (mm)	0.20 x 0.17 x 0.04
F (000)	992
θ range for data collection (°)	$3.16 \leq \theta \leq 24.99$
Index ranges (h, k, l)	$-10 \leq h \leq 11$
	$-15 \leq k \leq 15$
	$-19 \leq l \leq 21$
Reflections collected/unique (R_{int})	20502/3776(0.0291)
Max. and min. transmission	0.9963 and 0.9817
Data/restraints/parameters	3776/1/326
Goodness–of–fit on F^2	0.941
Final R indices [$I>2\sigma(I)$]	$R_1 = 0.0261$, w$R_2 = 0.0601$
R indices (all data)	$R_1 = 0.0310$, w$R_2 = 0.0612$
Largest peak and hole (e Å^{-3})	0.158, –0.133

Table S2. Selected bond lengths (Å) and angles (°) for Hqui.

Bond Lengths		Bond Angles	
N1–C15	1.359(2) / 1.362(2)	C15–N1–C16	122.78(12) / 122.97(12)
N1–C16	1.371(2) / 1.368(2)	O2–C13–C14	120.59(14) / 120.04(14)
O1–C14	1.370(2) / 1.357(2)	O2–C13–C17	122.91(13) / 123.10(13)
O2–C13	1.274(2) / 1.275(2)	C14–C13–C17	116.49(13) / 116.83(12)
C13–C14	1.418(2) / 1.417(2)	O1–C14–C15	118.84(13) / 118.63(13)
C13–C17	1.441(2) / 1.443(2)	O1–C14–C13	119.31(13) / 119.24(13)
C14–C15	1.377(2) / 1.382(2)	C15–C14–C13	121.74(14) / 122.05(14)
C15–C22	1.484(2) / 1.474(2)	N1–C15–C14	119.50(13) / 119.03(14)
C16–C21	1.405(2) / 1.404(2)	N1–C15–C22	116.30(13) / 116.66(13)
C16–C17	1.406(2) / 1.410(2)	C14–C15–C22	124.15(14) / 124.25(14)
C17–C18	1.413(2) / 1.403(2)	N1–C16–C21	120.37(13) / 120.31(13)
C18–C19	1.365(2) / 1.366(2)	N1–C16–C17	119.04(13) / 119.54(14)
C19–C20	1.401(2) / 1.408(2)	C21–C16–C17	120.57(13) / 120.16(14)
C20–C21	1.363(2) / 1.367(2)	C16–C17–C18	117.98(13) / 118.14(14)
C22–C23	1.391(2) / 1.393(2)	C16–C17–C13	119.99(13) / 119.43(14)
C22–C27	1.391(2) / 1.389(2)	C18–C17–C13	122.03(13) / 122.42(13)
C23–C24	1.384(2) / 1.378(2)	C19–C18–C17	120.90(14) / 121.31(14)
C24–C25	1.381(2) / 1.385(3)	C18–C19–C20	120.1(2) / 120.0(2)
C25–C26	1.382(2) / 1.379(3)	C21–C20–C19	120.77(14) / 120.2(2)
C26–C27	1.386(2) / 1.384(2)	C20–C21–C16	119.63(14) / 120.11(14)
		C23–C22–C27	119.32(14) / 118.48(14)
		C23–C22–C15	120.23(14) / 120.51(14)
		C27–C22–C15	120.45(14) / 121.01(14)

C24–C23–C22	120.2(2) / 120.5(2)
C25–C24–C23	120.2(2) / 120.6(2)
C24–C25–C26	120.0(2) / 119.5(2)
C25–C26–C27	120.1(2) / 120.1(2)
C26–C27–C22	120.1(2) / 120.9(2)

Table S3. Selected interatomic parameters (Å, °) of the hydrogen bonds of Hqui and complexes **2** and **3**.

D−H···A	*d*(D−H)	*d*(H···A)	*d*(D···A)	< (DHA)
Hqui				
O1A−H1B···O2	0.84	1.96	2.696(2)	146.2
O1−H1···O2A	0.84	2.05	2.843(2)	158.3
N1−H1A···O2A[i]	0.88	1.92	2.788(2)	166.7
N1A−H1AA···O2[ii]	0.88	2.12	2.905(2)	148.7
C18A–H18B···C23	0.95	2.723(2)	3.634(2)	160.88(10)
C18A–H18B···C23	0.95	2.828(2)	3.577(2)	136.47(10)
C19–H19A···C20A	0.95	2.888(2)	3.649(2)	137.93(10)
C20–H20A···C19A	0.95	2.851(2)	3.611(2)	137.66(10)
C21–H21A···O2A	0.95	2.6265(10)	3.337(2)	132.26(10)
C23–H23A···O1	0.95	2.6865(11)	3.574(2)	155.71(10)
C24A–H24B···N1	0.95	2.6816(12)	3.487(2)	142.97(11)
C24A–H24B···C16	0.95	2.682(2)	3.542(2)	150.78(11)
C27A–H27B···C24	0.95	2.592(2)	3.480(2)	155.68(11)
C13···C21			3.342(2)	
C13A···C20A			3.354(2)	
C13A···C21A			3.257(2)	
C14A···C21A			3.219(2)	
C18···C24A			3.191(2)	
*Complex **2***				
N1–H1···O5	0.880	2.034(2)	2.876(3)	159.63(14)
O6−H1W···O4	0.810(2)	2.051(2)	2.852(3)	170.0(3)
C3−H3A···O6	0.95	2.633(3)	3.388(4)	136.9(2)

C9−H9A···O5	0.95	2.546(2)	3.480(4)	167.5(2)
C12−H12A···O6	0.95	2.484(3)	3.433(4)	178.7(2)
C18−H18A···C24	0.95	2.761(2)	3.492(3)	134.3(2)
C20−H20A···O4	0.95	2.538(2)	3.396(4)	150.5(2)
C21−H21A···O5	0.95	2.420(2)	3.184(3)	137.3(2)
C23−H23A···O3	0.95	2.447(3)	3.082(4)	124.1(2)
C23−H23A···O5	0.95	2.552(2)	3.326(4)	138.8(2)
C24−H24A···C1	0.95	2.837(2)	3.576(3)	135.3(2)
C25−H25A···O1	0.95	2.5922(13)	3.542(2)	176.5(2)
C25−H25A···C27	0.95	2.865(2)	3.413(3)	117.76(14)
C26−H26A···C23	0.95	2.892(2)	3.744(4)	149.8(2)
C2···C20			3.375(3)	
C4···C20			3.324(4)	
C6···C16			3.398(3)	
C8···O5			3.175(3)	
C21···O5			3.184(3)	
C27···O2			3.175(3)	
*Complex **3a***				
N1−H1B···O3	0.88	2.12	2.983(4)	165.0
N4−H4B···O5^{i}	0.88	2.07	2.841(4)	146.5
C7−H7A···O4	0.95	2.438(2)	3.332(5)	156.7(2)
C9−H9A···O4	0.95	2.398(2)	3.343(4)	172.6(2)
C20−H20A···C3	0.95	2.870(4)	3.675(5)	143.1(2)
C20−H20A···O4	0.95	2.701(2)	3.314(4)	122.9(2)
C21−H21A···O5	0.95	2.332(2)	3.265(4)	164.2(2)

C23−H23A···C18	0.95	2.857(3)	3.687(5)	146.6(2)
C27−H27A···O2	0.95	2.622(2)	3.468(4)	148.6(2)
C2···C6			3.250(5)	
C4···C5			3.332(5)	
C13···C14			3.380(5)	
C16···C17			3.369(5)	
C16···C21			3.333(5)	

Symmetry codes for Hqui: (i) –0.5 + x, 0.5 – y, z; (ii) 0.5 + x, 1.5 – y, z.

Symmetry code for complex **3a**: (i) –1 + x, 1 – y, –0.5 + z

Table S4. The photograph, depicting the electrophoreogram, and tabulated data of the integrated densities characterizing the cleavage of pUC19 DNA with the reference compound $FeSO_4$ in different concentrations. Lane 1, a mixture of standard proteins; lane 2, control; lane 3, the linearized plasmid (L); lanes 4–21, the studied compound.

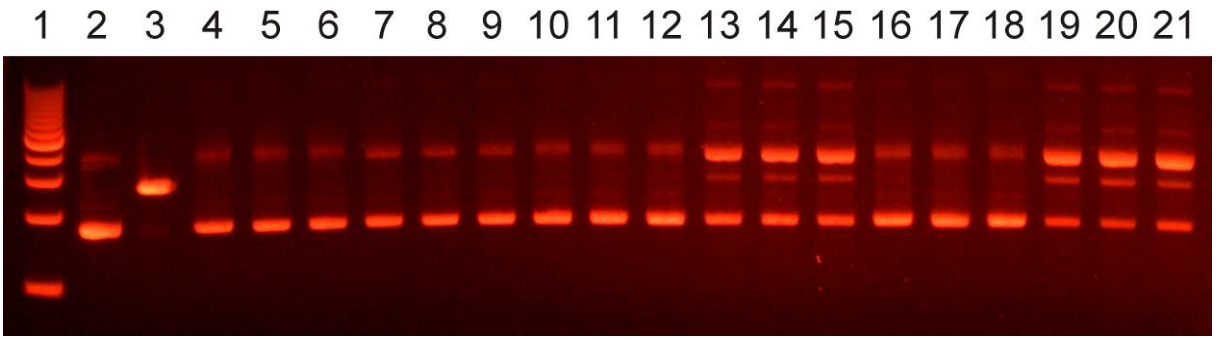

Lane	Conc. (μM)		CCC [AUC]	L [AUC]	OC [AUC]	DNA cleavage	Aver. DNA cleavage	SD
2 (control)			2 863	0	383	11.8	11.8	0
4	20	w/o ascorbate	1 918	0	458	19.3	18.2	0.92
5	20	w/o ascorbate	1 946	0	414	17.5		
6	20	w/o ascorbate	1 857	0	404	17.9		
7	20	with ascorbate	1 687	0	540	24.2	21.4	2.53
8	20	with ascorbate	1 752	0	425	19.5		
9	20	with ascorbate	1 860	0	474	20.3		
10	100	w/o ascorbate	2 102	0	463	18.1	18.1	0.12
11	100	w/o ascorbate	2 160	0	481	18.2		
12	100	w/o ascorbate	2 230	0	489	18.0		
13	100	with ascorbate	1 622	287	1 866	60.1	62.3	4.07
14	100	with ascorbate	1 602	293	1 803	59.9		
15	100	with ascorbate	1 307	345	1 965	67.0		
16	200	w/o ascorbate	2 072	0	546	20.9	19.1	1.92
17	200	w/o ascorbate	2 152	0	522	19.5		
18	200	w/o ascorbate	2 109	0	434	17.1		
19	200	with ascorbate	886	454	2 163	77.6	79.0	2.12
20	200	with ascorbate	731	483	2 236	81.4		
21	200	with ascorbate	913	449	2 321	77.9		

* supercoiled double-strand DNA
** open circular form of plasmid
† area under the curve

Table S5. The photograph, depicting the electrophoreogram, and tabulated data of the integrated densities characterizing the cleavage of pUC19 DNA with complex **1** in different concentrations. Lane 1, a mixture of standard proteins; lane 2, control; lane 3, the linearized plasmid (L); lanes 4–21, the studied compound.

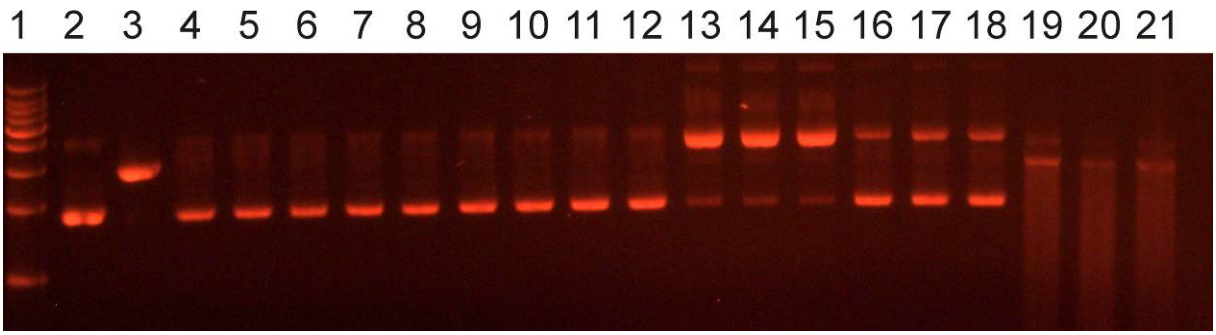

Lane	Conc. (μM)		CCC* [AUC]†	L [AUC]	OC** [AUC]	DNA cleavage	Aver. DNA cleavage	SD
2 (control)			1 731	0	180	9.4	9.4	0
4	20	w/o ascorbate	987	0	176	15.1	15.5	1.15
5	20	w/o ascorbate	1 046	0	179	14.6		
6	20	w/o ascorbate	1 000	0	202	16.8		
7	20	with ascorbate	1 118	0	191	14.6	15.3	1.56
8	20	with ascorbate	1 189	0	196	14.2		
9	20	with ascorbate	1 149	0	236	17.0		
10	100	w/o ascorbate	1 262	0	230	15.4	16.9	1.47
11	100	w/o ascorbate	1 425	0	289	16.9		
12	100	w/o ascorbate	1 468	0	330	18.4		
13	100	with ascorbate	268	0	2 059	88.5	89.1	0.83
14	100	with ascorbate	249	0	1 962	88.7		
15	100	with ascorbate	206	0	1 862	90.0		
16	200	w/o ascorbate	1 256	0	458	26.7	32.0	4.58
17	200	w/o ascorbate	1 224	0	656	34.9		
18	200	w/o ascorbate	1 239	0	649	34.4		
19	200	with ascorbate	smear	smear	smear		smear	
20	200	with ascorbate	smear	smear	smear			
21	200	with ascorbate	smear	smear	smear			

* supercoiled double-strand DNA
** open circular form of plasmid
† area under the curve

Table S6. The photograph, depicting the electrophoreogram, and tabulated data of the integrated densities characterizing the cleavage of pUC19 DNA with complex **3** in different concentrations. Lane 1, a mixture of standard proteins; lane 2, control; lane 3, the linearized plasmid (L); lanes 4–21, the studied compound.

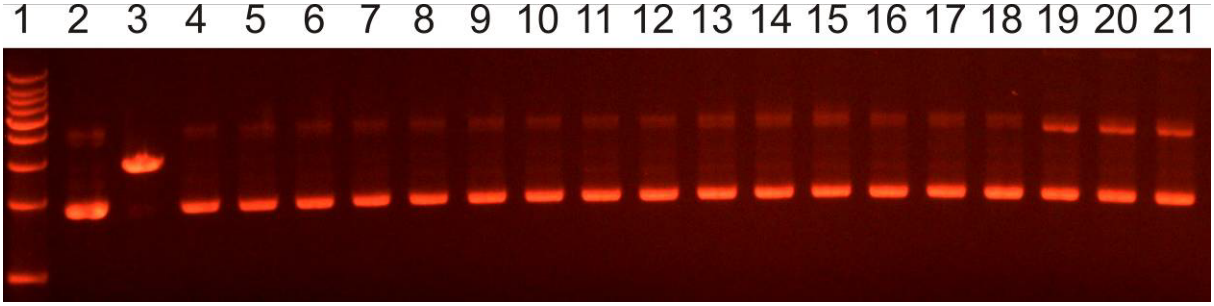

Lane	Conc. (μM)		CCC* [AUC]†	L [AUC]	OC** [AUC]	DNA cleavage	Aver. DNA cleavage	SD
2 (control)			2 302	0	351	13.2	13.2	0
4	20	w/o ascorbate	1 642	0	171	9.4	12.1	2.34
5	20	w/o ascorbate	1 547	0	250	13.9		
6	20	w/o ascorbate	1 611	0	237	12.8		
7	20	with ascorbate	1 620	0	243	13.0	14.2	1.41
8	20	with ascorbate	1 579	0	251	13.7		
9	20	with ascorbate	1 759	0	329	15.8		
10	100	w/o ascorbate	1 653	0	259	13.5	13.2	0.32
11	100	w/o ascorbate	1 721	0	256	12.9		
12	100	w/o ascorbate	1 735	0	260	13.0		
13	100	with ascorbate	1 810	0	331	15.5	17.6	1.88
14	100	with ascorbate	1 755	0	399	18.5		
15	100	with ascorbate	1 739	0	405	18.9		
16	200	w/o ascorbate	1 811	0	323	15.1	14.9	1.89
17	200	w/o ascorbate	1 852	0	369	16.6		
18	200	w/o ascorbate	1 855	0	274	12.9		
19	200	with ascorbate	1 749	0	665	27.5	28.1	0.52
20	200	with ascorbate	1 742	0	697	28.6		
21	200	with ascorbate	1 766	0	693	28.2		

* supercoiled double-strand DNA
** open circular form of plasmid
† area under the curve

Table S7. The photograph, depicting the electrophoreogram, and tabulated data of the integrated densities characterizing the cleavage of pUC19 DNA with complex **2** in different concentrations. Lane 1, a mixture of standard proteins; lane 2, control; lane 3, the linearized plasmid (L); lanes 4–21, the studied compound.

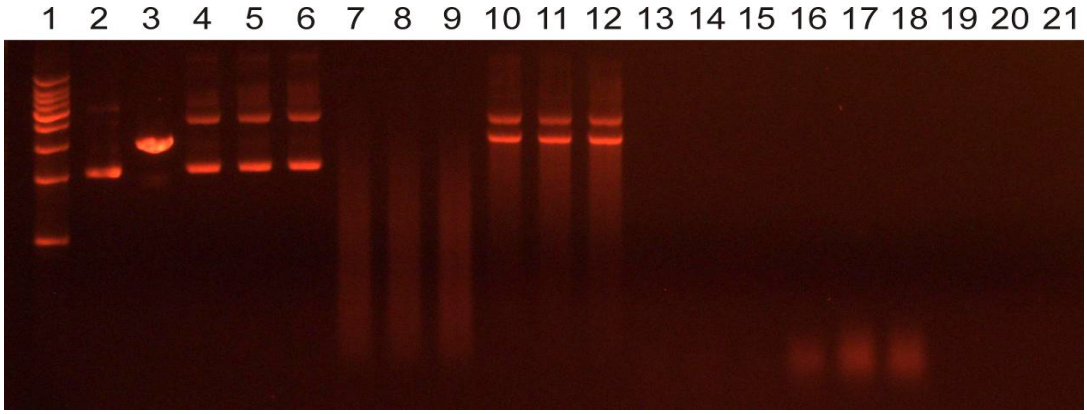

Lane	Conc. (μM)		CCC* [AUC]†	L [AUC]	OC** [AUC]	DNA cleavage	Aver. DNA cleavage	SD
2 (control)			2 717	0	105	3.86	3.86	0
4	20	w/o ascorbate	1 229	0	568	46.22	49.01	3.43
5	20	w/o ascorbate	1 230	0	650	52.85		
6	20	w/o ascorbate	1 357	0	651	47.97		
7	20	with ascorbate	smear	smear	smear		smear	
8	20	with ascorbate	smear	smear	smear			
9	20	with ascorbate	smear	smear	smear			
10	100	w/o ascorbate	0	1 155	739	100	100	0
11	100	w/o ascorbate	0	1 086	602	100		
12	100	w/o ascorbate	0	1 130	748	100		
13	100	with ascorbate	0	0	0		complete	
14	100	with ascorbate	0	0	0		cleavage	
15	100	with ascorbate	0	0	0			
16	200	w/o ascorbate	0	0	0		complete	
17	200	w/o ascorbate	0	0	0		cleavage	
18	200	w/o ascorbate	0	0	0			
19	200	with ascorbate	0	0	0		complete	
20	200	with ascorbate	0	0	0		cleavage	
21	200	with ascorbate	0	0	0			

* supercoiled double-strand DNA
** open circular form of plasmid
† area under the curve

Table S8. The photograph, depicting the electrophoreogram, and tabulated data of the integrated densities characterizing the cleavage of pUC19 DNA with complex **4** in different concentrations. Lane 1, a mixture of standard proteins; lane 2, control; lane 3, the linearized plasmid (L); lanes 4–21, the studied compound.

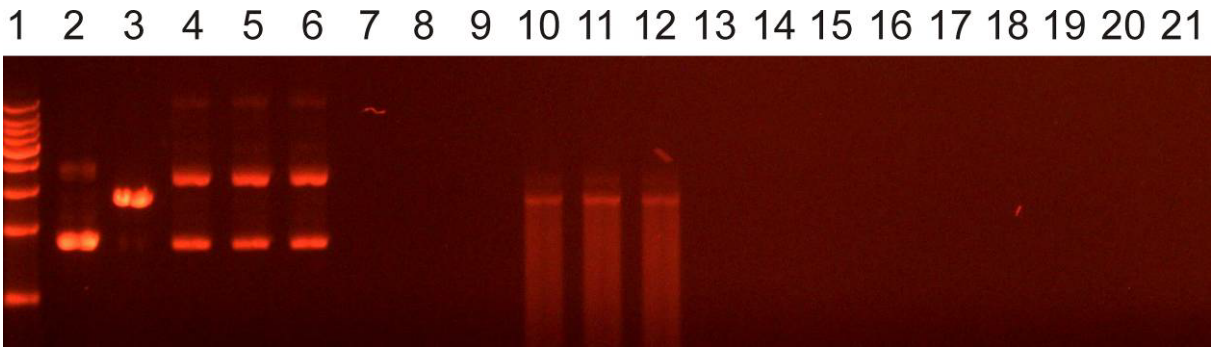

Lane	Conc. (μM)		CCC* [AUC]†	L [AUC]	OC** [AUC]	DNA cleavage	Aver. DNA cleavage	SD
2 (control)			2 302	0	351	13.2	13.2	0
4	20	w/o ascorbate	1 257	0	1 254	49.9	51.6	2.56
5	20	w/o ascorbate	1 123	0	1 346	54.5		
6	20	w/o ascorbate	1 256	0	1 269	50.3		
7	20	with ascorbate	0	0	0		complete	
8	20	with ascorbate	0	0	0		cleavage	
9	20	with ascorbate	0	0	0			
10	100	w/o ascorbate	smear	smear	smear		smear	
11	100	w/o ascorbate	smear	smear	smear			
12	100	w/o ascorbate	smear	smear	smear			
13	100	with ascorbate	0	0	0		complete	
14	100	with ascorbate	0	0	0		cleavage	
15	100	with ascorbate	0	0	0			
16	200	w/o ascorbate	0	0	0		complete	
17	200	w/o ascorbate	0	0	0		cleavage	
18	200	w/o ascorbate	0	0	0			
19	200	with ascorbate	0	0	0		complete	
20	200	with ascorbate	0	0	0		cleavage	
21	200	with ascorbate	0	0	0			

* supercoiled double-strand DNA
** open circular form of plasmid
† area under the curve

Table S9. The photograph, depicting the electrophoreogram, and tabulated data of the integrated densities characterizing the cleavage of pUC19 DNA with complex **5** in different concentrations. Lane 1, a mixture of standard proteins; lane 2, control; lane 3, the linearized plasmid (L); lanes 4–21, the studied compound.

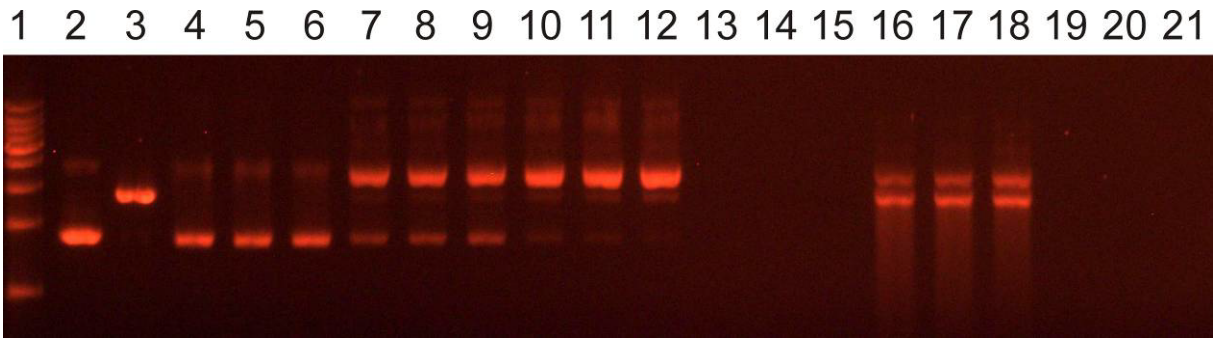

Lane	Conc. (μM)		CCC* [AUC]†	L [AUC]	OC** [AUC]	DNA cleavage	Aver. DNA cleavage	SD
2 (control)			1 731	0	180	9.4	9.4	0
4	20	w/o ascorbate	1 218	0	234	16.1	18.1	2.51
5	20	w/o ascorbate	1 155	0	242	17.3		
6	20	w/o ascorbate	1 204	0	319	20.9		
7	20	with ascorbate	416	128	1 429	80.2	78.9	1.35
8	20	with ascorbate	449	139	1 424	79.1		
9	20	with ascorbate	486	119	1 438	77.5		
10	100	w/o ascorbate	145	118	1 837	93.5	95.6	2.29
11	100	w/o ascorbate	111	166	1 969	95.4		
12	100	w/o ascorbate	53	178	2 282	98.0		
13	100	with ascorbate	0	0	0		complete	
14	100	with ascorbate	0	0	0		cleavage	
15	100	with ascorbate	0	0	0			
16	200	w/o ascorbate	0	856	580	100.0	100.0	0
17	200	w/o ascorbate	0	968	626	100.0		
18	200	w/o ascorbate	0	1 022	895	100.0		
19	200	with ascorbate	0	0	0		complete	
20	200	with ascorbate	0	0	0		cleavage	
21	200	with ascorbate	0	0	0			

* supercoiled double-strand DNA
** open circular form of plasmid
† area under the curve

Table S10. The photograph, depicting the electrophoreogram, and tabulated data of the integrated densities characterizing the cleavage of pUC19 DNA with complex **6** in different concentrations. Lane 1, a mixture of standard proteins; lane 2, control; lane 3, the linearized plasmid (L); lanes 4–21, the studied compound.

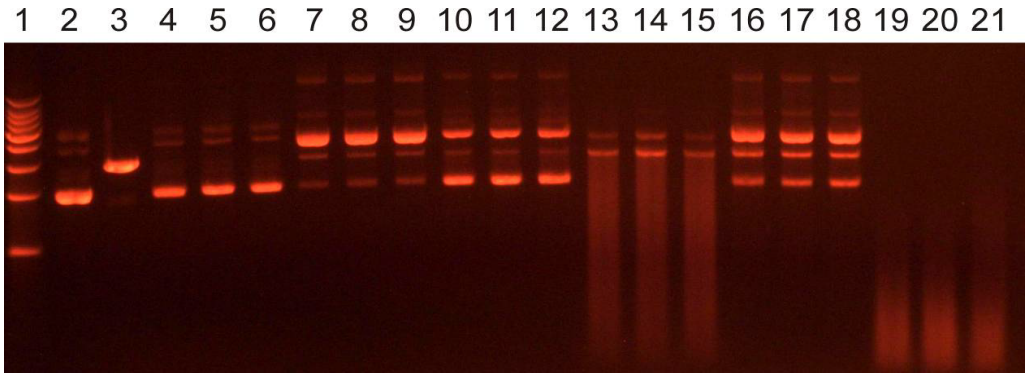

Lane	Conc. (μM)		CCC* [AUC]†	L [AUC]	OC** [AUC]	DNA cleavage	Aver. DNA cleavage	SD
2 (control)			2 397	0	132	5.2	5.2	0
4	20	w/o ascorbate	1 815	0	218	10.7	10.3	0.38
5	20	w/o ascorbate	1 863	0	206	10.0		
6	20	w/o ascorbate	1 797	0	206	10.3		
7	20	with ascorbate	250	323	2 414	92.4	90.5	1.67
8	20	with ascorbate	320	223	2 289	89.5		
9	20	with ascorbate	333	246	2 374	89.6		
10	100	w/o ascorbate	1 748	191	1 130	46.4	47.6	1.02
11	100	w/o ascorbate	1 763	202	1 233	48.1		
12	100	w/o ascorbate	1 612	192	1 112	48.1		
13	100	with ascorbate	smear	smear	smear		smear	
14	100	with ascorbate	smear	smear	smear			
15	100	with ascorbate	smear	smear	smear			
16	200	w/o ascorbate	769	721	2 092	82.1	80.4	1.62
17	200	w/o ascorbate	786	637	1 932	80.3		
18	200	w/o ascorbate	895	699	1 950	78.9		
19	200	with ascorbate	0	0	0		complete	
20	200	with ascorbate	0	0	0		cleavage	
21	200	with ascorbate	0	0	0			

* supercoiled double-strand DNA
** open circular form of plasmid
† area under the curve